

## Preparation of zirconia-modified epoxy acrylate emulsion and its application in waterborne anticorrosion coating

Shaoliang Li<sup>1,2,3</sup>, Xin Zhang<sup>1,2,3</sup>, Wenjuan Qu<sup>1,2,3,\*</sup>, Lijie Wang<sup>1,2,3</sup>, Houwei Li<sup>1,2,3</sup>, Jiabin Liu<sup>1,2,3</sup>

<sup>1</sup> College of Environment and Safety Engineering, Qingdao University of Science and Technology, Qingdao, 266042, P. R. China

<sup>2</sup> Shandong Engineering Research Center for Marine Environment Corrosion and Safety Protection, Qingdao University of Science and Technology, Qingdao, 266042, P. R. China

<sup>3</sup> Shandong Engineering Technology Research Center for Advanced Coating, Qingdao University of Science and Technology, Qingdao, 266042, P. R. China

\*E-mail: [qwj\\_710@163.com](mailto:qwj_710@163.com)

Received: 15 September 2021 / Accepted: 4 October 2021 / Published: 6 December 2021

---

Zirconia-modified epoxy acrylate emulsion was synthesized via soap-free emulsion polymerization by adding different amounts of modified ZrO<sub>2</sub> nanoparticles. The modified ZrO<sub>2</sub> nanoparticles were characterized by Fourier transform infrared spectroscopy (FTIR), X-ray diffraction spectroscopy (XRD) and scanning electron microscopy (SEM). Thermogravimetric analysis (TGA) indicated that the addition of modified ZrO<sub>2</sub> could improve the thermal stability of the films formed by the emulsions. Moreover, the electrochemical impedance spectra (EIS) results showed that the film former of zirconia-modified epoxy acrylate emulsion could effectively improve the corrosion resistance of the coatings. The results showed that the emulsion containing 1% modified ZrO<sub>2</sub> had the best thermal stability and the corresponding coating had the best corrosion resistance.

---

**Keywords:** Epoxy coatings; Zirconia; Nanoparticles; Corrosion

### 1. INTRODUCTION

As the backbone of human civilizations, the corrosion of metals and their alloys has always been a concern of the material industry, it is particularly important to protect them from corrosion [1,2]. Therefore, coatings have been widely applied to the metal substrates to protect them against corrosion [3,4]. Waterborne epoxy coating has attracted extensive attention in the field of metal protection due to its pollution free feature that is in accordance with the sustainable development [5]. Despite the above advantages, the application of waterborne epoxy coatings often has disadvantages such as poor barrier properties, leading to electrochemical corrosion [6], which greatly restricts its application in high

performance coatings. In recent years, due to the continuous development of nano-modification technology, the application of nano-modification in coatings has made great progress [7-9]. The compactness of the coating was improved through the correlative reaction between nanoparticles and epoxy resin and the catalytic action on the cross-linking reaction of epoxy resin. In addition, a large number of micro-pores are often formed during the production of the coating, especially the curing solvent coating, which causes the solvent to evaporate at high temperature, resulting in the corrosion resistance of the coating. This problem can be effectively solved by the addition of nanomaterials to form composite coatings, because the nanomaterials can eliminate the internal stress during epoxy curing [10]. Nanomaterials also can enter the coating through micro-pores and form an effective corrosive dielectric barrier [11].

Nano zirconium oxide has high strength, high modulus, high hardness and high fracture toughness [12] along with excellent wear resistance properties, good chemical resistance and low thermal conductivity [13]. It is a typical material with thermal and chemical stability. Moreover, it is one of the most promising nanomaterials in anticorrosive coatings. Modified  $ZrO_2$  nanoparticles can improve the compatibility and dispersion of nanomaterials in the coating materials. Therefore, it is usually necessary to modify the surface of nanomaterials [14], and the functionalization of organic silane coupling agent is a very ideal way [15]. M. Behzadnasab used amino propyl trimethoxy silane (APS) to surface treat the nanoparticles in order to achieve proper dispersion of the nanoparticles in the epoxy-based coating and to enable the nanoparticles to chemically interact with the polymeric coating [16]. Shenglin Liu chose  $\gamma$ -(2, 3-propylene oxide) propyl trimethoxysilane (KH-560) to modify the surface of  $ZrO_2$ , GO and  $ZrO_2 + GO$  hybrids. And the corrosion resistance of pure Zinc/Aluminum (Zn/Al) coatings, Zn/Al +  $ZrO_2$  coatings, Zn/Al + GO coatings and Zn/Al +  $ZrO_2 + GO$  coatings were studied and compared [17]. Although nanomaterials as physical fillers in waterborne epoxy coating had been widely studied in the field of anticorrosion, the introduction of nanomaterials by chemical action through grafting copolymerization is rarely studied.

In this paper,  $\gamma$ -aminopropyl triethoxysilane (KH-550) was selected to modify the surface of  $ZrO_2$ . Then the self-made epoxy acrylate emulsion was modified by grafting copolymerization with functionalized  $ZrO_2$ , and the waterborne epoxy coating was prepared by using it as the main film former. The structure of functionalized  $ZrO_2$  was analyzed by FT-IR, XRD and SEM. Additionally, the thermal stability was studied by thermogravimetric analysis (TGA). Then waterborne epoxy coatings with different amounts of modified  $ZrO_2$  were prepared, and the corrosion resistance of the coatings was analyzed by EIS.

## 2. EXPERIMENTAL

### 2.1. Materials

Nanometer zirconia ( $ZrO_2$ ) was received from Xuancheng Jingrui New Material Co., Ltd. 3-aminopropyltriethoxysilane (KH550), absolute ethanol, titanium pigment and barium sulfate powder

were purchased from Sinopharm Chemical Reagent Co.,Ltd. Deionized water and epoxy acrylate emulsion was prepared in our laboratory.

## 2.2. Preparation of modified $ZrO_2$ and its modification to epoxy acrylate emulsion

The  $ZrO_2$  (30wt.% in water) was added into the four-necked flask, which was placed with a stirrer. Install the four-necked flask containing the sample into a constant temperature water bath of 70°C. Next, KH-550 was slowly added into the flask under mechanical stirring and then stirred for 6h at 70°C. The modified zirconia was obtained. The modified  $ZrO_2$  was slowly added after the heat preservation reaction of self-made epoxy acrylate emulsion. The modified  $ZrO_2$  content varied (0%, 0.5%, 1%, 3% and 5%), and the resulting materials were labelled Z-0, Z-0.5, Z1-1, Z-3 and Z-5, respectively.

## 2.3. Preparation of waterborne anticorrosion coatings

A certain amount of deionized water, barium sulfate powder, titanium pigment and related additives were stirred for 15min at the speed of 1000r/min, and then the color paste prepared was poured into the cone mill for full grinding. The color paste was added to the emulsion prepared above and dispersed for 10min, and then the corresponding additives were added to disperse for 30min, the  $ZrO_2$  modified epoxy acrylate waterborne anticorrosion coatings were obtained. According to the emulsion added (Z-0, Z-0.5, Z-1, Z-3 and Z-5), waterborne anticorrosion coatings were labeled as C-0, C-0.5, C-1, C-3 and C-5, respectively.

## 2.4. Characterizations

X-ray diffraction (XRD) patterns were performed by the Bruker D8 Advance diffractometer (Rigaku Japan) with 4 s per step operating at 30 mA, 35 kV at  $2\theta$  from 5 to 90° by using Cu  $K\alpha$  radiation in the reflection mode and step size of 0.075°. Fourier transform infrared (FT-IR) was performed on a Nicolet IS10 Thermo Scientific spectrophotometer (Waltham, MA, USA) with the KBr pellet technique. The spectra were recorded in the absorption mode in the 3600–600  $cm^{-1}$  regions with resolution of 4  $cm^{-1}$  and average of 32 scans. The structural morphology of the  $ZrO_2$  and modified  $ZrO_2$  by scanning electron microscope (SEM) using a S-4800 instrument (Hitachi Corp., Tokyo, Japan). Thermogravimetry analysis (TGA) was performed at a heating rate of 20°C/min from 50°C to 700°C by using a TGA/SDTA 851 thermobalance from Mettler Toledo, Inc. (Schwerzenbach, Switzerland). All electrochemical measurements were carried out using the Parstat 4000 workstation obtained from AMETEK and equipped with a classical three-electrode system, and the electrochemical tests were conducted in 3.5 wt.% NaCl aqueous solution at room temperature. The electrochemical impedance spectroscopy (EIS) spectra was obtained by using the three electrochemical cell arrangement, the Q235B carbon steel electrode with coating, a saturated calomel electrode (SCE) and a platinum plate were used as working electrode, reference electrode and counter electrode, respectively. The samples were immersed into 3.5 wt.% NaCl solution for 20 minutes to reach the purpose of steady open circuit potential (OCP) before the electrochemical tests. Prior to the potentiodynamic polarization curves

measurement, the EIS was performed in a frequency range from 100 KHz to 10 mHz and measured with a sinusoidal potential perturbation of 10 mV (peak to peak). The EIS data were analyzed on the basis of equivalent circuits fitted by the ZSimpWin software.

### 3. RESULTS AND DISCUSSION

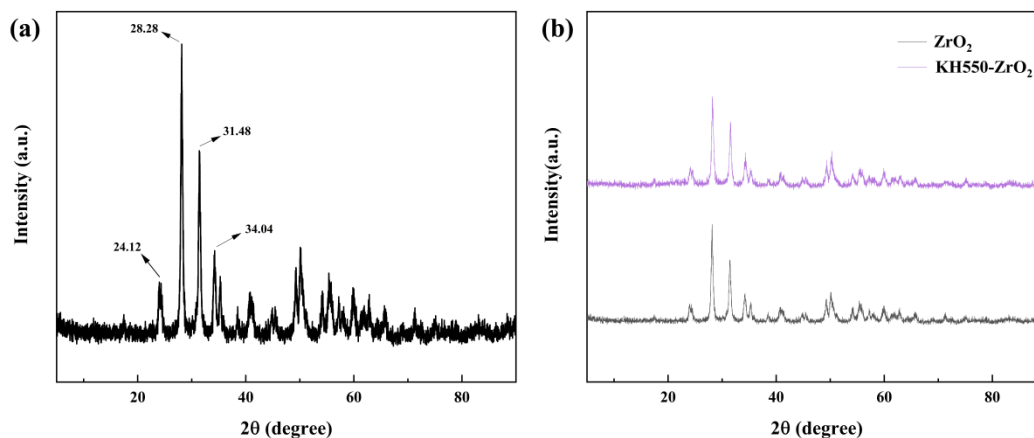


**Figure 1.** (a) XRD pattern of ZrO<sub>2</sub>, (b) XRD pattern of ZrO<sub>2</sub> and ZrO<sub>2</sub> modified by KH-550

Fig. 1 depicted the XRD pattern of sample. According to the XRD results in Fig. 1 (a), the diffraction peaks at 24.12, 28.28, 31.48 and 34.04° are the diffraction peaks of ZrO<sub>2</sub>, and the crystal structure is monoclinic, which is a typical ZrO<sub>2</sub> crystal structure. It can be seen from Fig. 1 (b) their diffraction peaks and intensity are basically same, indicating that the crystalline structure of ZrO<sub>2</sub> modified by KH-550 is not changed.

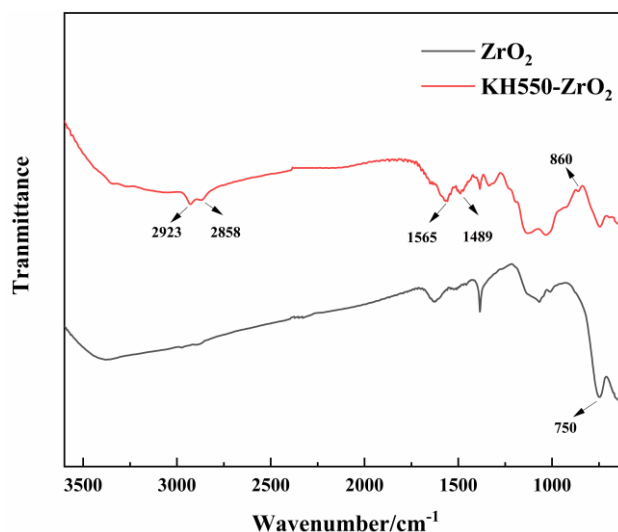


**Figure 2.** The FT-IR spectra of ZrO<sub>2</sub> and ZrO<sub>2</sub> modified by KH-550

Fig. 2 shows the FTIR spectra of ZrO<sub>2</sub>, as well as ZrO<sub>2</sub> modified by KH-550. The bands at region 2923 cm<sup>-1</sup> and 2858 cm<sup>-1</sup> assigned to alkyl groups [-(CH<sub>2</sub>)<sub>n</sub>-] appeared, the peak at 2923 cm<sup>-1</sup>

is the methylene asymmetric stretching vibration peak, and the  $2858\text{ cm}^{-1}$  is the methyl symmetric stretching vibration peak, indicating the existence of KH-550 on the surface of  $\text{ZrO}_2$  [18]. The peaks detected near  $1565\text{ cm}^{-1}$  and  $1489\text{ cm}^{-1}$  are attributed to the amino characteristic bimodal, from the aminopropyl on KH-550. The peak position of Zr-O-Si band at  $860\text{ cm}^{-1}$  shows that KH-550 has successfully bonded with  $\text{ZrO}_2$  by reaction between the hydroxy groups of KH-550 and the oxyethyl groups of  $\text{ZrO}_2$  [19]. The peak at  $750\text{ cm}^{-1}$  corresponded to the peak of Zr-O-Zr, which is the  $\text{ZrO}_2$  characteristic peak [20].

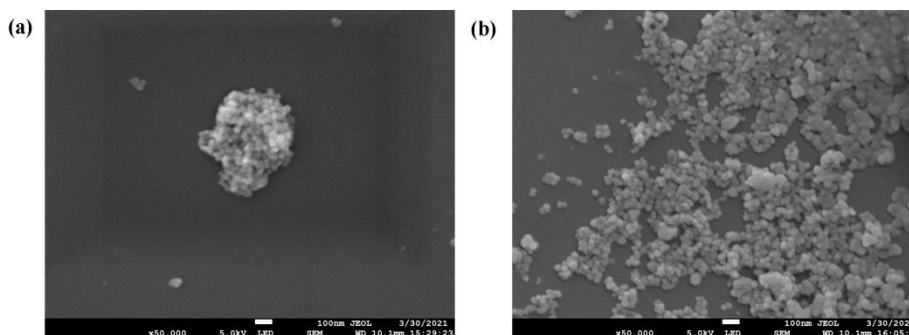


**Figure 3.** (a) SEM images of  $\text{ZrO}_2$  (a) SEM images of  $\text{ZrO}_2$  modified by KH-550

Fig. 3 shows SEM images of  $\text{ZrO}_2$  and  $\text{ZrO}_2$  modified by KH-550. It can be seen that the unmodified  $\text{ZrO}_2$  has poor dispersion and serious agglomeration. Furthermore, the particles adhered to each other and showed massive distribution. On the contrary, the modified  $\text{ZrO}_2$  has good dispersibility, the distribution is more uniform, and the agglomeration phenomenon is obviously weakened. Through the comparison of Fig. 3 (a) and Fig. 3 (b), it can be seen that the dispersion property of modified  $\text{ZrO}_2$  has been significantly enhanced, which is beneficial to the subsequent experiments.

The thermal degradation behavior of the composites was evaluated by thermogravimetric analysis (TGA) [21]. Fig. 4 shows the TGA and DTG curves of films. Relevant thermal analysis data was presented in Table 1, the  $T_{\text{max}}$  represents the temperature of maximum weight loss rate [22].

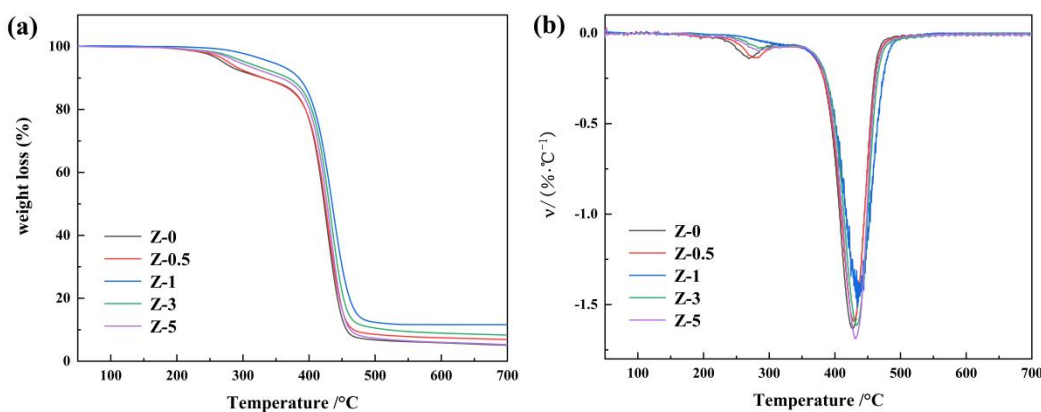


**Figure 4.** (a) TGA thermogram of films; Z-0, Z-0.5, Z-1, Z-3, Z-5. (b) DTG thermogram of films; Z-0, Z-0.5, Z-1, Z-3, Z-5.

Fig. 4 shows the thermal stability of Z-0, Z-0.5, Z-1, Z-3 and Z-5 latex. As is shown in Fig. 4 (a), the first stage was in the range of 240-340 °C with a small decomposition. The reason may be that the thermal decomposition of the epoxy resin. By comparing the five curves, it can be seen that when the amount of modified ZrO<sub>2</sub> is 1%, the weight loss of this process is the smallest, which is due to the graft reaction between modified ZrO<sub>2</sub> and epoxy resin. Moreover, the weight loss with modified ZrO<sub>2</sub> is generally lower than that without modified ZrO<sub>2</sub>. By comparing the curves of Z-0, Z-0.5 and Z-1, it can be seen that the char residue increases with the increase of the amount of modified ZrO<sub>2</sub>. By comparing the curves of Z-1, Z-3 and Z-5, it can be seen that the char residue decreases with the increase of the amount of modified ZrO<sub>2</sub>, and when the amount of modified ZrO<sub>2</sub> is 5%, the char residue is almost the same as that without modified ZrO<sub>2</sub>. This may be due to the graft reaction between the emulsion and the modified ZrO<sub>2</sub> when the modified ZrO<sub>2</sub> was added at the beginning, but with the increase of the added amount, the amount of modified ZrO<sub>2</sub> was too much, resulting in the gel phenomenon of the emulsion in the insulation reaction stage. The maximum amount of char residue increased by 228%, indicating that the addition of modified ZrO<sub>2</sub> improved the high temperature thermal stability of the emulsion. Meanwhile, it can be seen from Fig. 4 (b) that the temperature of maximum weight loss rate of the emulsion with modified ZrO<sub>2</sub> is generally higher than that of the emulsion without modified ZrO<sub>2</sub>, and the temperature corresponding to the maximum weight loss rate is the highest when the amount of modified ZrO<sub>2</sub> is 1%. The above results shows that the emulsion has better thermal stability at high temperature when the amount of modified ZrO<sub>2</sub> is 1%. More details on the quality changes and char residual are shown in Table 1.

**Table 1:** Thermogravimetric data of the films; Z-0, Z-0.5, Z-1, Z-3, Z-5.

	Z-0	Z-0.5	Z-1	Z-3	Z-5
<b>Weight loss in 240-340</b>	8.626%	8.351%	4.314%	6.292%	7.158%
<b>Char residue</b>	5.107%	6.879%	11.623%	8.301%	5.276%
<b>T<sub>max</sub></b>	426°C	429°C	434°C	433°C	431°C

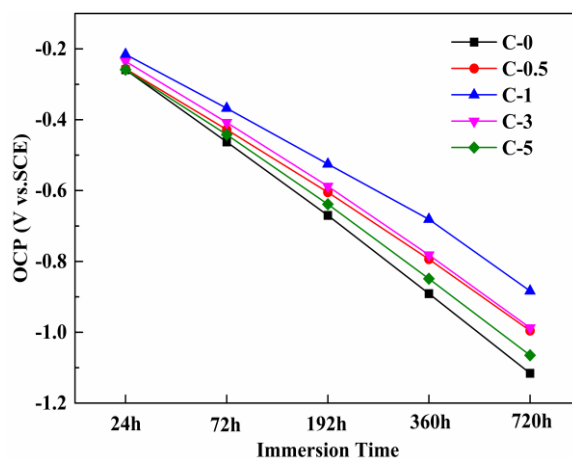


**Figure 5.** The OCP values of coatings at various immersion time

Open circuit potential (OCP) [23] is an important thermodynamic parameter in electrochemistry, which is used to characterize the corrosion probability of materials. Fig. 5 shown the change of  $E_{corr}$  of different coatings in 3.5wt.% NaCl solution with the change of immersion time.

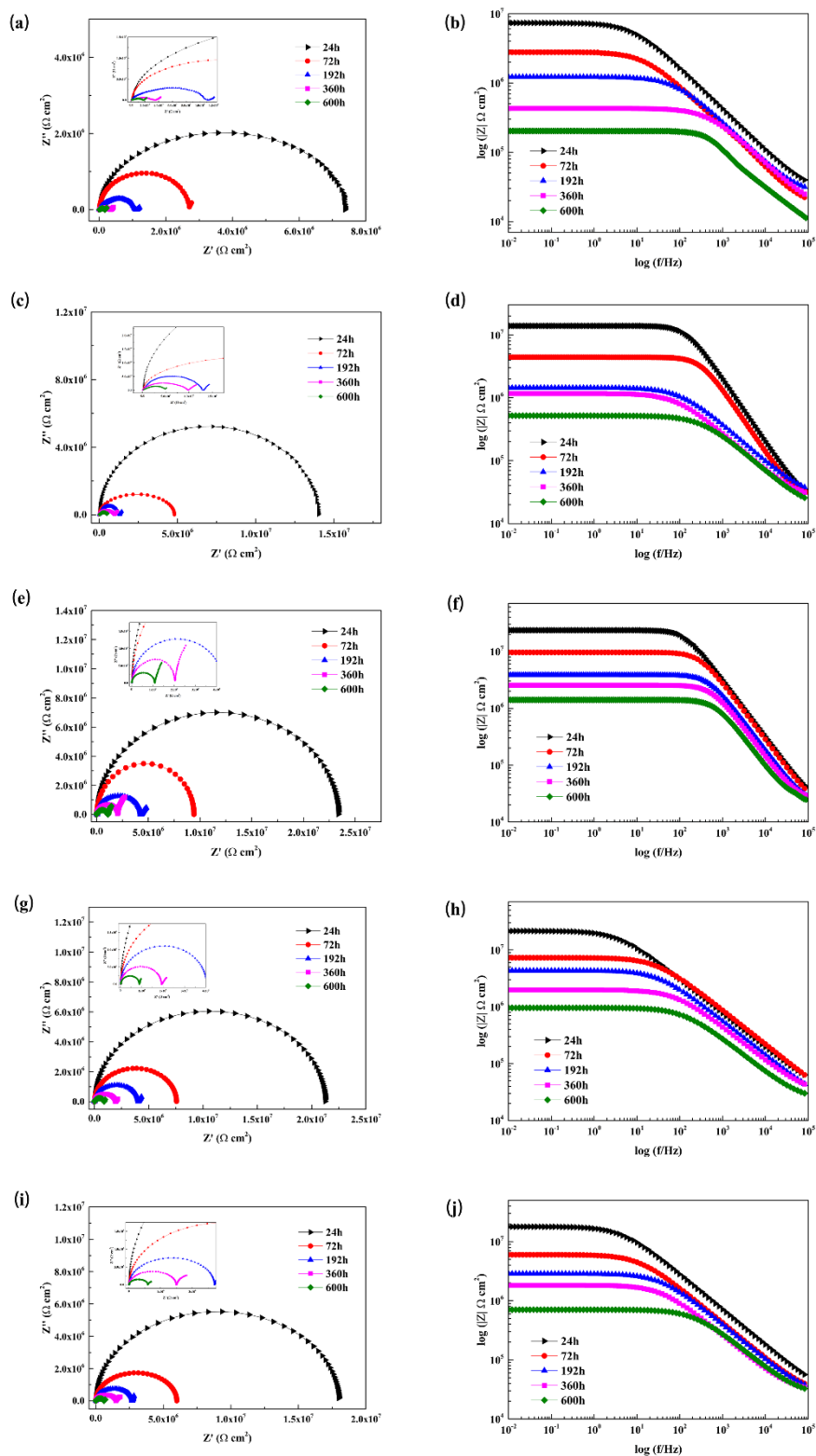


**Figure 6.** Nyquist and Bode diagrams of EIS measurements performed on different coatings C-0 (a, b), C-0.5 (c, d), C-1 (e, f), C-3 (g, h) and C-5 (i, j)

The OCP values of all samples were negative at the initial soaking stage, which may be caused by the reaction of waterborne epoxy coating with water. For some coating systems, the protective effect of coating on matrix can be judged by the change of open circuit potential. In general, if the coating is completely dense, the open circuit potential is almost unchanged. However, passivation layer has some corrosion. And the lower the open circuit potential is, the more severe the corrosion is. In other words, the lower the OCP value is, the higher the corrosion tendency is. As can be seen from the Fig. 5, the OCP value became lower and lower over time. This is mainly because that the coatings were eroded by corrosive medium. In addition, the comparison of the five curves shown that the OCP value of the coatings with  $ZrO_2$  was higher than that of the coatings without  $ZrO_2$  except at the initial soaking stage, indicating that the addition of  $ZrO_2$  can reduce the corrosion tendency of the coating. And the OCP value of C-1 coating was significantly higher than that of other coatings.

The anticorrosion ability and the electrochemical properties of coatings were also investigated by electrochemical impedance spectra (EIS) in 3.5 wt% NaCl solution [24]. Fig. 6 shows the Nyquist and Bode plots of different coatings immersed in 3.5 wt% NaCl solution for different hours. Comparing a, c, e, g and i in Fig. 6, it can be seen that two capacitive loops appeared in the figure a when the immersion time reached 72 hours, while in the rest of the figures the appearance of the two capacitive loops were observed after 72 hours of immersion time. This indicates that the time of C-0.5, C-1, C-3 and C-5 for the electrolyte to penetrate the film and reach the contact interface between the epoxy coating and the steel was longer than C-0, which also indicates that the addition of  $ZrO_2$  effectively retards the penetration of the electrolyte. Meanwhile, it can be seen from the Nyquist plots that the semicircular diameter of C-1 was the largest, that is, the corrosion resistance of C-1 was the best.

The Bode plot [25] is a graphical representation of the frequency response of a system. As shown in the bode plots, the initial (24h) impedance values for C-0, C-0.5, C-1, C-3 and C-5 were  $7.37 \times 10^6 \Omega \text{ cm}^2$ ,  $1.40 \times 10^7 \Omega \text{ cm}^2$ ,  $2.34 \times 10^7 \Omega \text{ cm}^2$ ,  $2.13 \times 10^7 \Omega \text{ cm}^2$  and  $1.80 \times 10^7 \Omega \text{ cm}^2$  respectively, which showed that the coating had a significant protective effect at this time. The final (600h) impedance values for C-0, C-0.5, C-1, C-3 and C-5 were  $2.05 \times 10^5 \Omega \text{ cm}^2$ ,  $1.16 \times 10^6 \Omega \text{ cm}^2$ ,  $1.42 \times 10^6 \Omega \text{ cm}^2$ ,  $9.67 \times 10^5 \Omega \text{ cm}^2$  and  $7.06 \times 10^5 \Omega \text{ cm}^2$  respectively. At the same time, it can be seen from the Bode plot that the impedance values of each coating were gradually getting smaller as the immersion time increases. Comparing all the bode plots above, the impedance value of the coatings (Fig. 6. d, f, h and j) with  $ZrO_2$  were significantly higher than that of the coating (Fig. 6. b) without the addition of  $ZrO_2$ , which indicates that the addition of  $ZrO_2$  significantly improves the corrosion resistance of the coating. Moreover, the impedance values of C-1 coating for each different immersion time is higher than the other coatings. This also indicates that C-1 has the best corrosion resistance.

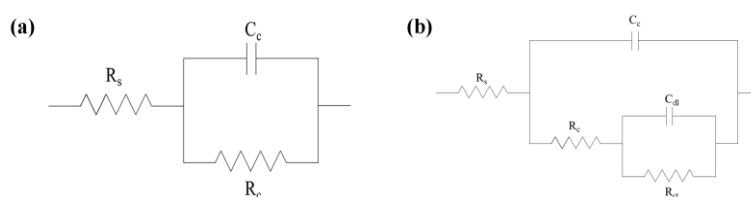


**Figure 7.** electrical equivalent circuit models

The equivalent circuit model was developed using ZSimpWin software, and the equivalent circuit (EEC) [26] shown in Fig. 7 was used to interpret the impedance response, and the optimal numerical fits of all EIS results were obtained [27,28]. The solution resistance between the working electrode and the reference electrode, the pore resistance of the plating, the charge transfer resistance between the steel surface and the solution interface, the capacitance of the plating, and the double layer capacitance between the steel surface and the electrolyte interface correspond to the five parts of the EEC,  $R_s$ ,  $R_c$ ,  $R_{ct}$ ,  $C_c$ , and  $C_{dl}$ , respectively [29,30]. Model a (Fig. 7. a) was used when the electrolyte solution did not permeate the membrane, i.e., when the C-0 coating was immersed for 24 h and when the C-0.5, C-1, C-3 and C-5 coatings were immersed for 72 h. Model 2 was used in other cases (Fig. 7. b).

From the above analysis, it is clear that the addition of zirconium oxide can effectively improve the corrosion resistance of the coating. On the one hand,  $ZrO_2$  can enter the micro-pores produced during the production of coatings and form an effective barrier of corrosive media. On the other hand,  $ZrO_2$  modified by KH-550 can interact with the epoxy group of epoxy resin and play a catalytic role in the cross-linking reaction of epoxy resin. This can effectively improve the denseness of the coating, which in turn can play a role in improving the corrosion resistance. In addition, as the addition of zirconium oxide increases, the corrosion resistance of the coating was significantly improved. However, when the addition of zirconium oxide was too high, it caused the gelation phenomenon of the emulsion, which led to a decrease in the corrosion resistance of the coating. The results showed that the best corrosion resistance of the coating was achieved when the addition amount of  $ZrO_2$  was 1%.

#### 4. CONCLUSIONS

In the current study,  $ZrO_2$  was successfully modified and different amounts of emulsion and coating were prepared. The addition of  $ZrO_2$  had a significant effect on the thermal stability of the emulsions and the anticorrosive properties of the coating. The morphology and structure of  $ZrO_2$  were characterized by scanning electron microscope (SEM), Fourier transform infrared (FTIR) spectroscopy and X-ray diffraction (XRD). The results confirmed that KH-550 successfully surface functionalized  $ZrO_2$  and significantly improved its dispersion. The thermogravimetric analysis indicated that the addition of  $ZrO_2$  could improve the thermal stability of the films formed by the emulsions, and the best thermal stability of the film was obtained when the addition of  $ZrO_2$  was 1%. Moreover, the electrochemical impedance spectra (EIS) results showed that the addition of  $ZrO_2$  could effectively improve the corrosion resistance of the coatings. But the excess of modified  $ZrO_2$  in zirconia-modified epoxy acrylate emulsion had some negative effects on the corrosion resistance. Therefore, the coating with 1% modified  $ZrO_2$  in emulsion possessed the best anticorrosion performance.

#### ACKNOWLEDGEMENTS

This work was financially supported by the Major Science and Technology Innovation Program of Shandong Province, China (No.2019JZZY010821) and the National Natural Science Foundation of China (Grant No. 21975138).

## References

1. N. Jadhav, C.A. Vetter and V.J. Gelling, *Electrochim. Acta*, 102 (2013) 28–43.
2. K. Gong, M. Wu, F. Xie, G.X. Liu and D.X. Sun, *Mater. Chem. Phys.*, 270 (2021) 124826.
3. S. Niroumandrad, M. Rostami and B. Ramezanzadeh, *Prog. Org. Coat.*, 101 (2016) 486–501.
4. M.H. Jiang, Y.Z. Gao, S.A. Patil, H.Q. Hou, W. Feng and S.L. Chen, *J. Power Sources*, 491 (2021) 229595.
5. F.J. Xiao, C. Qian, M.Y. Guo, J.Z. Wang, X.R. Yan, H.L. Li and L. Yue, *Prog. Org. Coat.*, 125 (2018) 79–88.
6. N. Wang, H.Y. Gao, J. Zhang, L. Li, X.L. Fan and X.L. Diao, *Prog. Org. Coat.*, 135 (2019) 74–81.
7. H.L. Ma, X. Zhang, F.F. Ju and S.-B. Tsai, *Sci. Rep.*, 8 (2018) 3045.
8. S. Wang, W.Q. Liu, H.Y. Shi, F.Y. Zhang, C.H. Liu, L.Y. Liang and K. Pi, *Polymer*, 222 (2021) 123665.
9. J.F. Chen, J.T. Zhang, M.J. Hu, Z.Q. Zheng, K.D. Wang and X.B. Li, *Surf. Coat. Technol.*, 353 (2018) 1–7.
10. W.B. Zhang, H.Y. Wang, C.J. Lv, X.X. Chen, Z.Q. Zhao, Y.Q. Qu and Y.J. Zhu, *Surf. Eng.*, 36 (2020) 175–183.
11. Y.J. Jing, P.Q. Wang, Q.B. Yang, Q.R. Wang and Y. Bai, *Colloids Surf. Physicochem. Eng. Asp.*, 608 (2021) 125625.
12. R. Medina, F. Hauptert and A.K. Schlarb, *J. Mater. Sci.*, 43 (2008) 3245–3252.
13. S. Halder, P.K. Ghosh and M.S. Goyat, *High Perform. Polym.*, 24 (2012) 331–341.
14. Y.-T. Lin, T.-M. Don, C.-J. Wong, F.-C. Meng, Y.-J. Lin, S.-Y. Lee, C.-F. Lee and W.-Y. Chiu, *Surf. Coat. Technol.*, 374 (2019) 1128–1138.
15. C.Y. Zhang and Y. Tian, *Eng. Struct.*, 185 (2019) 15–25.
16. M. Behzadnasab, S.M. Mirabedini, K. Kabiri and S. Jamali, *Corros. Sci.*, 53 (2011) 89–98.
17. S.L. Liu, Y.S. Zhu, X.P. Zheng, X.Y. Lai, R.N. Jia and X.S. Yuan, *Diam. Relat. Mater.*, 108 (2020) 107868.
18. M. Sabzi, S.M. Mirabedini, J. Zohuriaan-Mehr and M. Atai, *Prog. Org. Coat.*, 65 (2009) 222–228.
19. M. Behzadnasab, S.M. Mirabedini, K. Kabiri and S. Jamali, *Corros. Sci.*, 53 (2011) 89–98.
20. S.L. Liu, Y.S. Zhu, X.P. Zheng, X.Y. Lai, R.N. Jia and X. Yuan, *Diam. Relat. Mater.*, 108 (2020) 107868.
21. J.L. Li, H.Y. Wang and S.C. Li, *Polym. Degrad. Stab.*, 164 (2019) 36–45.
22. J.L. Li, H.Y. Wang and S.C. Li, *High Perform. Polym.*, 31 (2019) 1217–1225.
23. A. Kherfi, A. Madani, D. Chalal and S. Benidir, *Synth. Met.*, 277 (2021) 116795.
24. C.B. Hu, Y. Li, N. Zhang and Y.S. Ding, *RSC Adv.*, 7 (2017) 11732–11742.
25. S.X. Li, J.P. Wang, W.J. Qu, J.J. Cheng, Y.N. Lei, M. Liu and D. Wang, *J. Electrochem. Sci.*, (2019) 11641–11650.
26. S. Cruz-Manzo and P. Greenwood, *J. Electroanal. Chem.*, 892 (2021) 115270.
27. H.U. Nwankwo, L.O. Olasunkanmi and E.E. Ebenso, *Sci. Rep.*, 7 (2017) 2436.
28. J.L. Oliveira, *Prog. Org. Coat.* (2021) 11.
29. S.J. Yuan, B. Liang, Y. Zhao and S.O. Pehkonen, *Corros. Sci.*, 74 (2013) 353–366.
30. W. Kwon, J.-M. Kim and S.-W. Rhee, *Electrochim Acta*, 68 (2012) 110–113.